Proceedings of EuCoMeS, the first
European Conference on Mechanism Science
Obergurgl (Austria), February 21–26 2006
Manfred Husty and Hans-Peter Schröcker, editors

Towards a Predictive Model for Temperature-Induced Deformation of an Industrial Robot

Pranchalee Poonyapak* M. John D. Hayes*

The warm-up and cool-down behaviour of a KUKA KR-15/2 six-axis industrial robot for a particular task is measured and its effect on the robot repeatability determined. The robot is taught two poses. In each pose a tool-flange mounted laser points directly onto the CCD chip of a digital camera. The motion sequence is repeated for 15 hours (900 minutes) three different times at 30%, 75% and 10% of maximum robot speed. The temperature distribution history of the robot during the motion sequence is recorded with a thermal imaging camera. Temperature-induced robot dimension changes are estimated from the geometry of the camera positions and how the laser spot migrates across the CCD chip over time from start to end. The results from the 30% run are used to estimate linear coefficients of thermal expansion. These empirical estimates are in the same order of magnitude as the coefficient corresponding to the aluminium alloy that is the dominant material comprising the robot links. The empirical coefficient of thermal expansion from the 30% run is used to predict the measured deformations for the 75% and 10% runs.

Introduction

In this paper the first steps towards the development of a predictive model for compensating the temperature-induced deformations of serial robots in general, and a KUKA KR-15/2 industrial robot in particular, is presented. A critically important, and often overlooked, issue is that repeatability and accuracy are not constant throughout the entire volume of the workspace and that they vary over time, (ISO 9283:1998). Fluctuations arise from thermal expansion, stress and strain under applied loads, dimension errors, dynamic characteristics, and system errors of the controller inverse kinematics algorithms. The long-term goal of this work is to eliminate the warm-up cycle times needed when an industrial robot is not operated in a thermally stable condition. The thermal instability is induced by loses in the robot motors and gearboxes, and typically requires two hours of continuous motion through the reachable workspace at 100%

*Deptartment of Mechanical and Aerospace Engineering, Carleton University, ppoonyap@connect.carleton.ca, jhayes@mae.carleton.ca

motor speed in order to reach steady state. This warm-up cycle time carries with it a large cost on a production line. Moreover, if for some reason the robot workcell must go offline the resulting cool-down will have to be compensated by additional warm-up cycles. During the warm-up the workcell has zero productivity. The motivation for this work arises from the potential for increasing workcell productivity while simultaneously eliminating warm-up times and associated costs from production schedules.

Methods of robot kinematic calibration endeavor to improve the accuracy of the robot up to the level of its repeatability. There is a very broad spectrum of conceptual approaches to the problem in the existing literature, see for example (Hayati (1983); An et al. (1988); Sklar (1989); Bennett and Hollerbach (1991); Mooring et al. (1991); Vincze et al. (August, 1994); Wampler et al. (1995); Zhuang and Roth (1996); Gong et al. (2000); Hollerbach and Wampler (1996); Fratpietro and Hayes (June, 2004); Simpson and Hayes (June, 2004)). However, to the best of the authors knowledge, with the exception of investigation of temperature-induced errors in CNC machine tools (Großmann et al. (2004)), there exists little archival literature studying the contribution of temperature induced dimensional deformation in the robot kinematic geometry. Results of the work presented in this paper indicate that the repeatability of a KUKA KR-15/2 is nearly one order of magnitude better than the manufacture stated value of ± 100 μm when the robot is operated in a thermally stable condition, i.e., *warmed-up*. The implication is that if the drift can be compensated during operation of the robot then the repeatability is essentially improved. This, in turn, implies greater accuracy can be achieved through calibration.

To obtain an estimation of the positioning repeatability of a KUKA KR-15/2 robot, and hence the best-case estimation of positioning accuracy, an experiment was devised to estimate the drift in repeatability caused by heat transferred to the links via losses in the motors and gearboxes. The measurement system is optically-based and contactless. The robot repeats a motion sequence of two taught configurations for a period of about 15 hours. In each pose the robot points a laser diode directly onto a CCD camera chip, i.e., no lens. After visiting the two camera configurations, the robot presents itself to an infra-red camera for a temperature measurement. The experiment was run three separate times using three different limits for joint actuator motor speeds, 30%, 75% and 10% of maximum speed. The maximum speeds of each motor are listed in Table 1. The first and second runs were started with the robot at ambient room temperature. For the final run the robot was not allowed to cool down.

Table 1: KUKA KR-15/2 maximum joint rates.

Joint	1	2	3	4	5	6
Speed (deg/s)	152	152	152	284	293	604

From the joint angles used in changing the configuration to point to the next camera and from the laser position error, an overall view of the repeatability, and how it changes with temperature over time is observed. Moreover, empirical data that enable the temperature induced dimension changes to be predicted for a given task, its rate and duration of repetition is obtained. The long-term goal of this research is to establish a coefficient of thermal expansion for each link of the robot, taking into account the contribution of each motor and gearbox for a particular motion. With such a set of coefficients programmed into the controller warm-up and cool-down cycles could be eliminated thereby significantly enhancing the productivity of the robot.

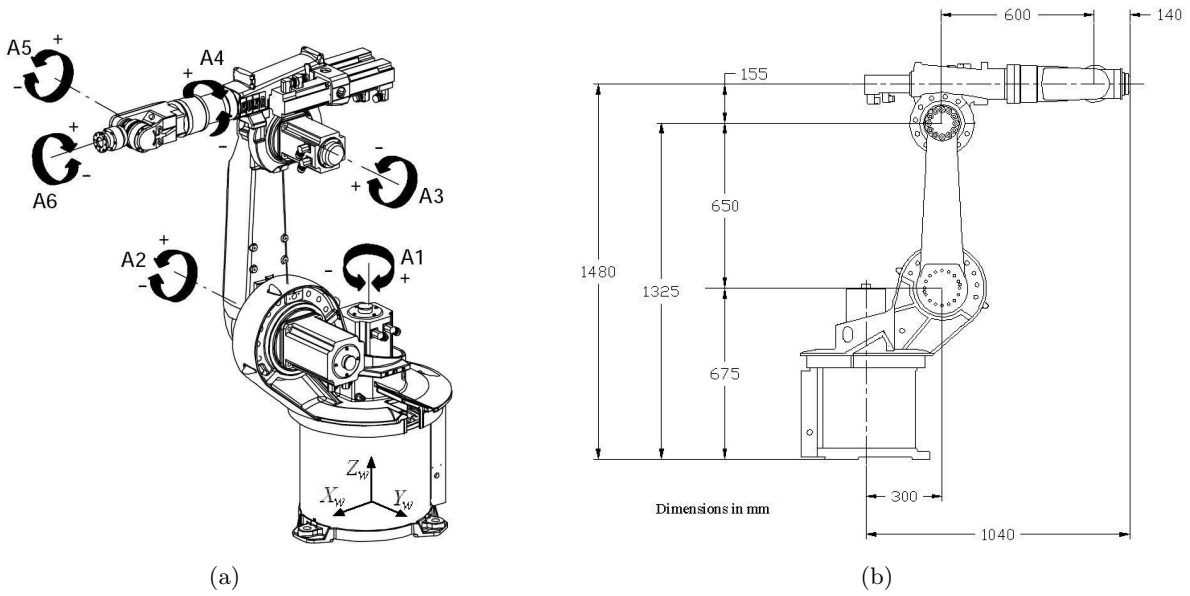

(a) (b)

Figure 1: KUKA KR-15/2, taken from Operating Handbook (KR15).

1 Apparatus

The robot used in this experiment was a KUKA KR-15/2. It is a wrist-partitioned robot with six actuated revolute axes. The axes, together with the base and tool reference coordinate frames, are illustrated in Figures 1. Its rated payload is 15 kg and the volume of its working envelope, using the wrist-centre (intersection of orthogonal axes 4, 5 and 6) as reference point, is approximately 13.1 m^3. The most important specification related to this experiment is the stated repeatability:

$$\text{repeatability} \quad = \quad \pm 100\ \mu\text{m}.$$

The measurement raw-data was obtained using the following equipment. The two CCD cameras were each a CCIR standard Pulnix TM-6CN with a cell size of 8.6(H)x8.3(V) μm, and resolution of 752(H)x582(V). Each camera was adjusted to manual gain control in field mode, with the following settings: gamma = 0.45; blacklevel = 0.1 mV; whitelevel = 0.7 mV; electronic shutter speed = 1/10000 s. The framegrabber was a National Instrument PCI-1409 monochrome.

The laser diode was made by Schaefter and Kirchhoff. It had a wavelength of 638 nm; and was tuned to be almost invisible.

Temperature measurements were obtained using an FSI FLIR SC 500 ThermoVision Uncooled Infrared Camera. The detector is a Focal Plane Array (FPA), uncooled microbolometer with resolution of 320×240 pixels and thermal sensitivity of 0.1°C at 30°C. Its temperature range is -20°C to 120°C, with an accuracy of ±2°C full scale.

1.1 CCD Camera Placement

Two CCD cameras, A and B, were placed in the workspace such that the geometric centres of the CCD arrays have coordinates in Frame $\{W\}$ listed in Table 2. When the robot points the laser

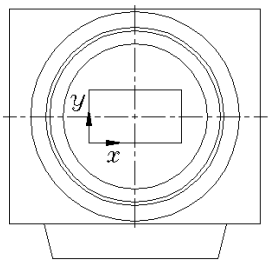

Figure 2: CCD chip reference coordinates.

towards Camera A, or B, the corresponding configuration is called *Pose A*, or *B*, respectively. The corresponding tool flange centre coordinates are also listed in Table 2. The CCD camera reference coordinate origin and basis directions are illustrated in Figure 2. This figure is a schematic drawing of the front view of the camera. The coordinates of the laser point in each of the three camera images are with respect to the corresponding camera coordinate system.

Table 2: Coordinates of Camera A and B CCD chip centres, and tool flange centre coordinates for Pose A and B all expressed in Frame $\{W\}$.

Camera	x_W (mm)	y_W (mm)	z_W (mm)	Pose	x_W (mm)	y_W (mm)	z_W (mm)
A	1017.20	-213.58	148.40	A	1087.78	-48.62	217.75
B	1016.20	-190.49	104.39	B	1087.33	-38.29	198.07

With the assumption that when the robot attains either of the two poses the first three links dominate the position error, only the first three joint angles are significant. This is a reasonable assumption for wrist-partitioned robots. The joint angles for Poses A and B are listed in Table 3. The length of the first three links is projected into the xy_W-plane using the nominal link lengths shown in Figure 1 and listed in Table 5 and relevant angles from Table 3.

The cameras were placed so that the camera coordinate planes were constrained with respect to the *world* coordinate frame of the robot, $\{W\}$, see Figures 1(a) and 3(a). The position and orientation of Frame $\{W\}$ are identical to that of the robot base frame, located within the fixed zeroth link of the robot, illustrated in Figures 1(a) and 3(a). Figure 3(b) shows a rendering of the cameras in their mounting brackets and the robot tool flange pointing the laser orthogonally onto Camera A.

Referring to Figure 3(a), the y-axis direction of each camera is parallel to the x_W-axis. The camera x-axis directions are different. To get a focused image of the laser on the chip the distance had to be 106 mm for all measurements. Additionally, the laser was maintained nominally orthogonal relative to each CCD chip. Small deviations from perpendicular induce relatively large positioning errors that are not modelled. Regardless, these errors are believed to be unimportant at this proof-of-concept stage.

For Camera A, the CCD array plane, xy_A, is parallel to the world frame xz_W-plane, see Figure 3(a). For Camera B, the y_A and y_B axes have the same direction, but the x_B axis has been rotated about y_A by 9.1100°, see Figure 3(a).

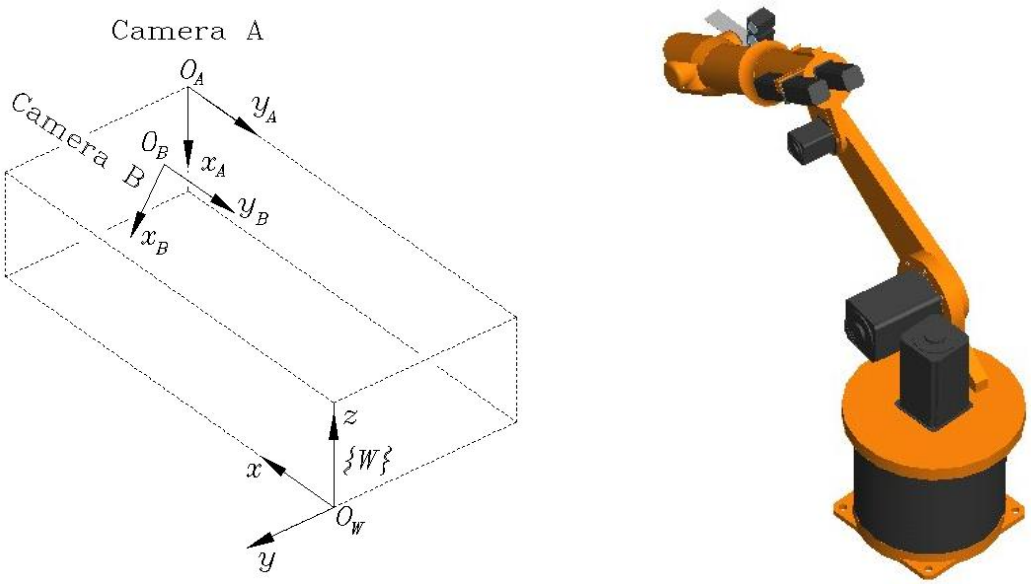

(a) (b)

Figure 3: Camera placement and kinematic configuration for Pose A.

1.2 Determination of Positioning Repeatability

The positioning repeatability in each camera plane was calculated from the positional variation of the laser spot on the CCD chip. Based on the pixel size, there is a pixel resolution of 8.6 μm. The estimated resolution provided by the two-dimensional COG-algorithm (see Ofner et al. (1999)) used for the evaluation is approximately 1 μm.

1.3 Measurement of Robot Temperature

The temperature history of the robot during the measurement run was recorded with the infrared camera. The thermal images corresponding to start and end times are shown in Figures 4. These figures are shown for illustrative purposes only. The relevant temperatures used for

Table 3: Joint angles for Pose A and B.

Joint	Pose A	Pose B
Axis	Joint angle (deg.)	Joint angle (deg.)
ϑ_1	4.2300	4.2300
ϑ_2	17.5462	17.5462
ϑ_3	-16.8840	-16.8840
ϑ_4	-89.5160	-89.5160
ϑ_5	-66.8551	-57.7451
ϑ_6	180.0000	180.0000

computation, which were extracted from the IR camera data, are listed in Table 4. Note, the hot spot visible on the nearly vertical arm of the robot Figure 4(a) and Figure 4(b) is the laser power supply. The resulting heating curves for different locations on the robot surface are all first-order exponential heating curves of the form $y = y_0 + Ae^{-(x/\tau)}$.

The changes in temperature, ΔT, of each run listed in Table 4 are the differences between the temperature of each link at the beginning of the run and the maximum temperature of each link at the end of the run. The highest temperature spot generally is located in the area close to the motor. The maximum ΔT measured from the experiment is used for computing the maximum Δl, the maximum change in length due to the change in temperature. The maximum drift of positioning repeatability is then obtained using the value of the maximum Δl.

For Runs 1 the robot was started at ambient temperature and run at 30 % maximum motor speed. The robot was allowed to cool for 10 hours before the start of Run 2. This was believed to be enough time to allow the robot links to cool to ambient conditions, however it was not the case. At the start of Run 2, where the maximum motor speed was 75% of maximum, the average link temperature was 1°C greater than at the start of Run 1. For Run 3 the robot was not allowed to cool down. It ran at 10% maximum velocity and the cool-down history, instead of the warm-up history, was recorded.

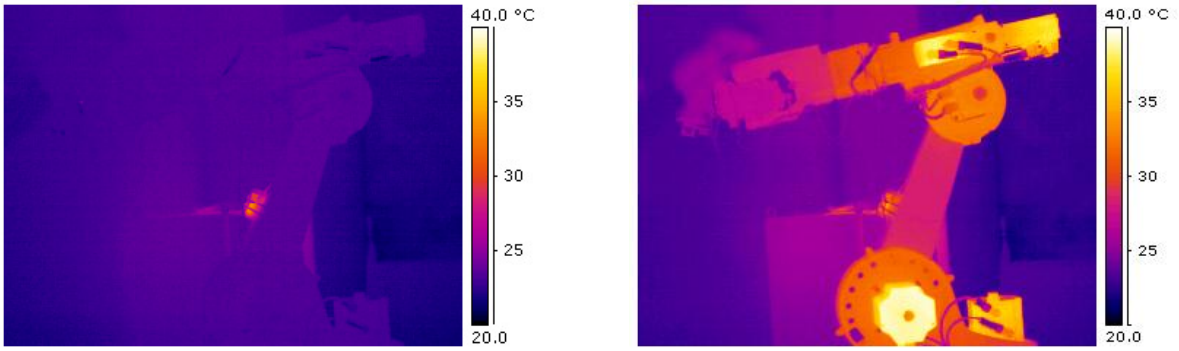

(a) Start. (b) End.

Figure 4: Thermal images of the robot at start and end of measurements for Run 1 (shown for illustrative purposes only and not for temperature data extraction).

2 Results

With reference to Figures 6, it can be seen that

$$l \quad = \quad (l_2 \cos 17.55 + l_3 \cos 55.57). \tag{1}$$

The length l is the norm of the position vector of the tool flange centre in Frame $\{W\}$. This length itself is then projected onto the y and x camera basis directions for deformation measurements. The effective lengths l_2 and l_3 include the portions of links 1, 2, and 3 that feel the effects of the heat transferred through the motor flanges at axes 1, 2, and 3.

Table 4: Temperature data and Δl_x from experiment.

Run	Time	Temperature (°C)				Δl_x (μm)	
		Link 2		Link 3		Camera A	Camera B
1 (30%)	start end	23.40 28.10	$\Delta T_2 = 4.70$	23.35 30.10	$\Delta T_3 = 6.75$	131	130
2 (75%)	start end	24.40 28.40	$\Delta T_2 = 4.00$	24.34 30.65	$\Delta T_3 = 6.30$	120	120
3 (10%)	start end	28.40 27.20	$\Delta T_2 = -1.20$	30.65 28.45	$\Delta T_3 = -2.20$	-40	-41

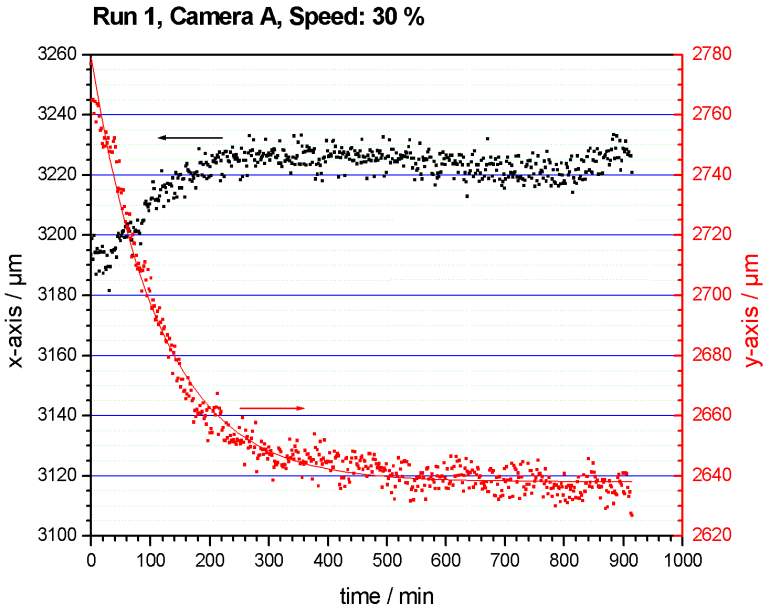

Figure 5: Center of laser spot on Camera A over measurement time for Run 1.

It is well known that a property of all metals is that dimensions vary linearly with temperature within a certain range. The linear coefficient of thermal expansion, α, is defined to be

$$\alpha = \frac{\Delta l}{l \Delta T}, \tag{2}$$

where l is the nominal length at a specific initial reference temperature, Δl is the change in length due to the change in temperature in degrees Kelvin (or Celcius), ΔT. The Δl_x listed in Table 4 are extracted from the laser spot migration measured along the y-axes of the cameras. For example, see the graph presented in Figure 5. Using Equations (1) and (2) leads to:

$$\Delta l_x = \alpha \left(l_2 \cos 17.55 \Delta T_2 + l_3 \cos 55.57 \Delta T_3 \right) \cos\phi \cos\theta. \tag{3}$$

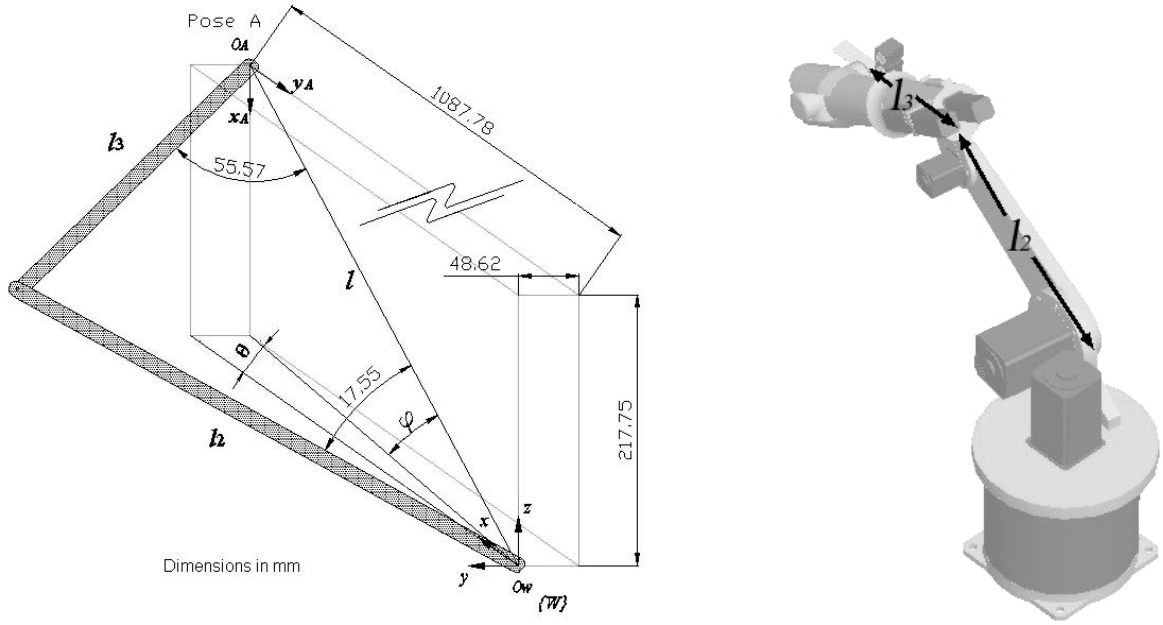

(a) (b)

Figure 6: Projected link length for Pose A.

Table 5: KUKA KR-15/2 *effective* link lengths at 23 ± 0.5°C.

Link	Length (m)	Description
2	$l_2 = 0.70$	Effective distance between Axes 2 and 3.
3	$l_3 = 0.78$	Effective distance between Axes 3 and 5.

From Run 1 data listed in Table 4, ΔT and Δl_x are obtained, while data from Table 2 and Figures 6 for Camera A yields l, $\phi = 11.31°$ and $\theta = 2.56°$ giving:

$$\begin{aligned} \alpha_A &= \frac{131.00 \times 10^{-6}}{(0.70 \cos 17.55 \cdot 4.70 + 0.78 \cos 55.57 \cdot 6.75) \cos 11.31 \cos 2.56}, \\ &= 21.87 \times 10^{-6}\ C^{-1}. \end{aligned}$$

For Camera B, $\phi = 10.32°$ and $\theta = 2.02°$ and similarly:

$$\alpha_B = 21.63 \times 10^{-6}\ {}^{\circ}C^{-1}.$$

The average apparent thermal expansion coefficient from Cameras A and B is

$$\overline{\alpha} = 21.75 \times 10^{-6}\ {}^{\circ}C^{-1}.$$

Table 6: Comparison of α_A, α_B, $\overline{\alpha}$ and $\alpha_{6061-T6}$.

	Coefficient($\times 10^{-6}\ C^{-1}$)
α_A	21.87
α_B	21.63
$\overline{\alpha}$	21.75
$\alpha_{6061-T6}$	23.20

Note: $\alpha_{6061-T6}$ is an average coefficient of 6061-T6 aluminium alloy, the dominant material comprising the robot links, in the temperature range 20°C to 100°C (Lampman (1990)).

2.1 Using the Coefficient of Thermal Expansion from Run 1 to Predict Δl of Runs 2 and 3

To start, α_A is used to predict Δl_x of measured using Camera A data. It was determined that $\alpha_A = 21.87 \times 10^{-6}\ ^\circ C^{-1}$. Using Equation (3) and data listed in Tables 4 and 5 yields:

$$\begin{aligned}\Delta l &= \alpha_A\ (l_2 \cos 17.55 \Delta T_2 + l_3 \cos 55.57 \Delta T_3) \cos 11.31 \cos 2.56 \\ &= 21.87 \times 10^{-6} (0.70 \cos 17.55 \cdot 5.00 + 0.78 \cos 55.57 \cdot 7.30) \cos 11.31 \cos 2.56 \\ &= 140.46 \times 10^{-6}\ m.\end{aligned}$$

Due to the result of incomplete cooling down between Runs 1 and 2, the start temperature of links 2 and 3 at the start of Run 2 were 1°C higher than those of Run 1. To compare the predicted Δl_x with experiment values of Δl_x from Run 2, an adjustment is required to account for the additional thermal expansion at the start of Run 2.

$$\begin{aligned}\Delta l_{x_{adjust}} &= 21.87 \times 10^{-6} (0.70 \cos 17.55 \cdot 1.00 + 0.78 \cos 55.57 \cdot 1.00) \cos 11.31 \cos 2.56 \\ &= 23.75 \times 10^{-6}\ m.\end{aligned}$$

Therefore, the actual value of Δl_x read at Run 2 experiment should be:

$$\begin{aligned}\Delta l_{x_{Run_2}} &= \Delta l_{x_{Run2_{exp}}} + \Delta l_{x_{adjust}} \\ &= 120.00 \times 10^{-6} + 23.75 \times 10^{-6} \\ &= 143.75 \times 10^{-6}\ m.\end{aligned}$$

For Run 3, the appropriate values from Tables 4 and 5 are used to obtain:

$$\begin{aligned}\Delta l_x &= 21.87 \times 10^{-6} (0.70 \cos 17.55 \cdot (-1.20) + 0.78 \cos 55.57 \cdot (-2.20)) \cos 11.31 \cos 2.56, \\ &= -37.94 \times 10^{-6}\ m\end{aligned}$$

Likewise, Δl_x from the Camera B measured data is predicted using α_B. As well, Δl_x from the Camera A and B measured data is predicted using $\overline{\alpha}$. Note that for the Camera B data, with a different camera location, the values of ϕ and θ are 10.32° and 2.02° respectively. All results are listed in Table 7.

Table 7: Δl_x and prediction error.

			Run 2	Run 3
$\alpha_{A\ CameraA}$	Δl_x (μm)	Predicted	140.46	-37.94
		Measured	143.75	-40.00
	%error		-2.29	-5.15
$\alpha_{B\ CameraB}$	Δl_x (μm)	Predicted	139.44	-37.67
		Measured	143.57	-41.00
	%error		-2.88	-8.12
$\overline{\alpha}_{\ CameraA}$	Δl_x (μm)	Predicted	139.69	-37.74
		Measured	143.62	-40.00
	%error		-2.74	-5.65
$\overline{\alpha}_{\ CameraB}$	Δl_x (μm)	Predicted	140.21	-37.88
		Measured	143.70	-41.00
	%error		-2.43	-7.61

3 Discussion

From Table 6, all computed α are less than that of 6061-T6 aluminium alloy. While 6061-T6 is the principal material, it is only one of several constituents of the links. The temperature change of each link occurs over 900 minutes and the thermal expansion and contraction occurs over that time. Due to the unsteady-state conditions, the computed α will be smaller than α of the 6061 quoted from the standard table in (Lampman (1990)). In addition, it is likely that parts of the structure set up conditions in which the links were further restrained from expansion and contraction. Careful examination of Table 7 reveals that the predicted temperature-induced deformation is consistently smaller that the actual deformation. For Run 2 the motor speed was increased from 30% to 75% of maximum motor speed. The resulting increased motor and gearbox losses result in a measured Δl_x of 120 μm in both Cameras, see Table 4. However, the average robot link temperature at the start of Run 2 was greater than at the start of Run 1. To compare the results, the measured values for Run 2 had to be adjusted by adding the expansion corresponding to a 1°C temperature increase. This means the thermal expansion, Δl_x, for Run 2 in Camera A is really 143.75 μm and in Camera B is 143.57 μm, as listed in Table 7.

For Run 3 the opposite trend is observed because of the thermal contraction associated with the overall temperature decrease caused by the 10% motor speed. Regardless, the trend in the predicted deformation is consistent; the predicted is less than the measured contraction. It is to be noted that the %error for Run 3 is consistently greater than that for Run 2. This may be explained by the fact that the deformation is on the order of -40 μm as opposed to 140 μm. This should be expected, though, because the deformation is much closer to the estimated sub-pixel measurement resolution of 1 μm.

Camera A data predicted by using the average coefficient of thermal expansion, $\overline{\alpha}$, has larger %error than the data predicted using α_A. However, the overall prediction for data of both cameras is more accurate using $\overline{\alpha}$. This suggests that $\overline{\alpha}$ gives adequate quality prediction of

Δl_x for basic approximation. Using only one value of α for all links simplifies mathematical models and reduces calculation time. For a prediction that requires higher level of accuracy, an individual coefficient of thermal expansion determined for each pose shall be used.

4 Conclusions

Coefficients of thermal expansion based on the deformation recorded by Cameras A and B were computed from Run 1. These were, in turn, used to predict the thermal deformation for Runs 2 and 3 using the measured temperatures. The next step in development of this predictive model is to establish how the torque requirements for generalized tool flange centre trajectories are converted to power losses and how those losses generate temperature gradients on the link surfaces. However, the predicted temperatures would have to be somehow verified. These results suggest thermal imaging provide effective and useful data.

Results show that when the temperature of the robot links approach steady state, so does the positioning repeatability. The change in position error exhibits first order exponential behavior in the x_W-axis (the y-axes of the cameras). The assumption that thermal expansion is easily observed longitudinally than radially is supported by this result; however, it may also be an artifact of the experiment's geometry. The effect is more complicated in the other directions and in fact these deviations are much smaller and therefore less significant.

Once the robot has warmed-up, its positioning repeatability was 80% better than the manufacturers stated repeatability. However, if the robot is operated starting from a cold state the repeatability is 40% worse than the specified value. It is noteworthy that no mention of such heating effects on robot performance can be found in the manufacturer supplied operating literature for the KUKA KR-15/2, see Operating Handbook (KR15). The major implication of these results is that if the thermal response of the robot for specific cyclic tasks is known, the expansion can be numerically predicted and compensated by the controller, eliminating the need to allow the robot to heat-up. If the predictive thermal expansion model were sufficiently accurate, the repeatability of the robot, the lower bound of its accuracy, could be improved thereby allowing the robot to perform consistently better than its manufacturing specifications.

Given the fact that repeatability is an important performance criterion that is largely glossed over by many manufacturers, experimental research in this area is very well justified. The measurement sequence should be reworked so that only one motor is used, thereby providing data on the heat-up contribution of each motor. Several runs at different speeds would be necessary. A predictive heat transfer model may then be based on the temperature history correlated with motion geometry and individual motor torque requirements. Investigations into active compensation of link length changes should be made.

5 Acknowledgements

The authors gratefully acknowledge the patience, skill, persistence, and equipment contributed by Paul O'Leary, Markus Leitner, Christian Sallinger, and Ronald Ofner of the Institute for Automation, MU Leoben, in helping to obtain the experimental data used in this paper.

References

ISO 9283:1998, Manipulating Industrial Robots - Performance Criteria and Related Test Methods, ISO Std. ISO 9283:1998(E), April 1998.

KR15 Technical Data: Operating Handbook, KR C1 Release 2.2, KUKA Roboter GmbH.

C. An, C. Atkeson, and J. Hollerbach. Model-Based Control of a Robot Manipulator. *The MIT Press, Cambridge, Massachusetts, U.S.A., 1988.*

D. Bennett and J. Hollerbach. "Autonomous Calibration of Single-Loop Closed Kinematic Chains Formed by Manipulators with Passive Endpoint Constraints". IEEE Trans. Rob. & Autom., *vol. 7: pages 597–606, 1991.*

A. Fratpietro and M. Hayes. "Relative Measurement for Kinematic Calibration Using Digital Image Processing". in Proc. CSME Forum 2004, *University of Western Ontario, London, ON., Canada, June, 2004.*

C. Gong, J. Yuan, and J. Ni. "A Self-Calibration Method for Robotic Measurement System". ASME Journal of Manufacturing Science and Engineering, *2000.*

K. Großmann, B. Wunderlich, and S. Szatmari. "Progress in Accuracy and Calibration of Parallel Kinematics". in Proc. Parallel Kinematic Machines in Research and Practise: the 4^{th} Chemnitz Parallel Kinematics Seminar *Chemnitz, Germany, pages 49–68, 2004.*

S. Hayati. "Robot Arm Geometric Link Parameter Estimation". Proc. 22nd IEEE Conf. on Decision and Control, *San Antonio, TX, pages 1477–1483, 1983.*

J. Hollerbach and C. Wampler. "The Calibration Index and Taxonomy for Robot Kinematic Calibration Methods". International Journal of Robotics Research, *vol. 15: pages 705–712, 1996.*

S. Lampman, editor. Metals Handbook, *tenth edition*, Volume 2 Properties Selection: Nonferrous Alloys and Special-purpose Materials. *ASM International, Metals Park, OH, 1990.*

B. Mooring, Z. Roth, and M. Driels. Fundamentals of Manipulator Calibration. *John Wiley and Sons, Inc., New York, NY, 1991.*

R. Ofner, P. O'Leary, and M. Leitner. A Collection of Algorithms for the Determination of Construction Points in the Measurement of 3D Geometries via Light-Sectioning. Wesic '99, 2nd Workshop on European Scientific and Industrial Collaboration promoting: Advanced Technologies in Manufacturing, Newport, South Wales, United Kingdom, *1999.*

N. Simpson and M. Hayes. "Simulation of Kinematic Calibration Procedure That Employs the Relative Measurement Concept". in Proc. CSME Forum 2004, *University of Western Ontario, London, ON, Canada, June, 2004.*

M. Sklar. "Geometric Calibration of Industrial Manipulators by Circle Point Analysis". in Proc. 2nd Conf. on Recent Advances in Robotics, *Boca Raton, FL, pages 178–202, 1989.*

M. Vincze, J. Prenniger, and H. Gander. A Laser Tracking System to Measure Position and Orientation of Robot End Effectors Under Motion. The International Journal of Robotics Research, *vol. 13, no. 4: pages 305–314, August, 1994.*

C. Wampler, J. Hollerbach, and T. Arai. "An Implicit Loop Method for Kinematic Calibration and its Application to Closed-Chain Mechanisms". IEEE Trans. Rob. & Autom., *vol. 11, no. 5: pages 710–724, 1995.*

H. Zhuang and Z. Roth. Camera-Aided Robot Calibration. *CRC Press, Boca Raton, FL, 1996.*